Angle- and Spectral-Dependent Light Scattering from Plasmonic Nanocups

Nicholas S. King,[†,⊥] Yang Li,[†,⊥] Ciceron Ayala-Orozco,[§,⊥] Travis Brannan,[†] Peter Nordlander,[†,‡,⊥,*] and Naomi J. Halas[†,‡,§,⊥,*]

[†]Department of Physics and Astronomy, [‡]Department of Electrical and Computer Engineering, [§]Department of Chemistry, and [⊥]Laboratory for Nanophotonics, Rice University, 6100 Main Street, Houston, Texas 77005, United States

ABSTRACT As optical frequency nanoantennas, reduced-symmetry plasmonic nanoparticles have light-scattering properties that depend strongly on geometry, orientation, and variations in dielectric environment. Here we investigate how these factors influence the spectral and angular dependence of light scattered by Au nanocups. A simple dielectric substrate causes the axial, electric dipole mode of the nanocup to deviate substantially from its characteristic $\cos^2\theta$ free space scattering profile, while the transverse, magnetic dipole mode remains remarkably insensitive to the presence of the substrate. Nanoscale irregularities of the nanocup rim and the local substrate permittivity have a surprisingly large effect on the spectral- and angle-dependent light-scattering properties of these structures.

KEYWORDS: plasmon · nanoantenna · nanoshell · nanocup · symmetry breaking · scattering

Plasmons, the collective electronic oscillations of metallic nanoparticles and nanostructures, are at the forefront of the development of nanoscale optics. The sensitivity of the properties of plasmonic nanoparticles to geometry, dielectric environment, and light polarization permits many degrees of freedom in the design of plasmonic structures for specific phenomena or applications. Excitation of the surface plasmons of metallic and metallodielectric nanoparticles generates intense, localized electromagnetic fields that enable processes such as surface-enhanced chemical spectroscopies.[1−5] Controlling the precise geometry and composition of individual[6−8] or collective arrangements[9,10] of plasmonic nanoparticles easily tunes the excitation energy of these oscillations through the visible and near-infrared regions of the electromagnetic spectrum for various applications. Plasmonic nanostructures can also serve to couple optical signals to planar devices, enhancing the performance of light-emitting diodes,[11] photodetectors,[12,13] and solar cells.[14,15] Learning how to design plasmonic structures for these applications requires a comprehensive understanding of how this class of nanostructures alters the light-scattering properties of planar substrates and, conversely, how planar substrates, as symmetry-breaking elements, alter the optical response of plasmonic nanostructures.[16−22]

Reduced-symmetry 3D nanostructures such as nanocups (also known as semishells), possessing both electric and magnetic plasmon modes, are important model systems for the study of the light-scattering properties of nanoparticles on planar substrates. Nanocups consist of a hemispherical shell of metal fabricated around a dielectric nanoparticle core and have been of increasing interest in recent studies of plasmonic nanostructures due to their unusual and unique light-scattering properties.[23−26] Nanocups possess both an electric, axial plasmon mode and a magnetic, transverse plasmon mode at two distinct and easily discernible resonant frequencies.[23] These two plasmon modes have been shown to possess distinct and very different light-scattering characteristics.[24] The transverse plasmon mode exhibits a unique light-bending property where incident light from a broad cone of input angles is scattered in a direction normal to the cup rim.[24,27−30] Similarly, the axial mode scatters light with the $\cos^2\theta$ angular dependence of a dipole scattering source aligned with the nanocup axis of symmetry. This new degree of freedom, not available in symmetric nanoparticles, is of particular interest for the coupling of light from free space into planar or other reduced-dimensionality structures.

In this series of experiments, we directly examine the angle-dependent light-scattering properties of nanocups on a planar substrate. To compare the light-scattering properties of these structures directly with those of the equivalent, fully spherical core−shell nanoparticles on the same type of substrate, we fabricate our nanocup structures directly from chemically synthesized

* Address correspondence to halas@rice.edu, nordland@rice.edu.

Received for review June 7, 2011 and accepted July 15, 2011.

Published online July 15, 2011
10.1021/nn202086u

nanoshells. This is accomplished by removing the top portion of the spherical shell layer using a reactive ion etching process. The scattering from a submonolayer of oriented nanocups demonstrates the ability of these structures to scatter light preferentially out of the incident beam path. While previous studies associate light-bending behavior with the transverse plasmon mode of the nanocup,[24] here we observe that, in the presence of a substrate, the axial plasmon mode can also possess light-refractive properties. The sensitivity of the angular scattering profile to nanometer-scale geometric irregularities of the nanocup rim, characteristic of the reactive ion etching process applied to nanoshells, is also observed. We also find that small changes in the dielectric permittivity of the substrate local to the nanoparticle can result in sizable effects on its light-scattering properties. Simulations of the nanoparticle–substrate system using the finite element method (FEM) allow us to deduce the physical origin of both spectral and angular shifts in the light-scattering properties observed in our experiments.

RESULTS AND DISCUSSION

Sample Fabrication. A submonolayer of nanocups was produced by first synthesizing $[r_1, r_2]$ = [60, 78] nm SiO_2/Au core–shell nanoshells by previously reported methods,[6,31] where the dimensions of the core and total nanoparticle radius were directly obtained from scanning electron microscopy (SEM) measurements. The nanoparticles were then deposited sparsely on dielectric substrates to minimize any contributions to the observed optical properties from coupled, adjacent nanoparticles. Glass and silicon substrates cleaned with a "piranha" solution (30% H_2O_2, 70% H_2SO_4) were first functionalized with a nanoscale poly(4-vinylpyridine) (PVP) layer to promote nanoparticle adhesion.[32] The substrates were then submerged in a dilute solution of synthesized nanoshells for 4 h to produce a submonolayer of nanoparticles with an average surface density of approximately 2 particles/μm^2 (4% surface coverage). Compared to a close-packed geometry (~53 μm^2 or 74% surface coverage), this density was experimentally verified to eliminate any detectable interparticle coupling effects in the scattering measurements. The nanoshells were reshaped into nanocups by removing the top portion of the gold shell *via* plasma etching in a commercial reactive ion etch (RIE) unit (TRION Minilock-Phantom III RIE). High-power argon ion bombardment physically ablated a specific portion of the Au shell from the upper surface of the nanoshells, leaving Au semishells with exposed silica cores oriented in the direction of the surface normal (Figure 1a) (see Methods).[33] A scanning electron microscope (FEI Quanta 400 SEM) was used to measure the particle density of nanoshells on the surface, as well as to verify the degree of etching of the individual nanostructures

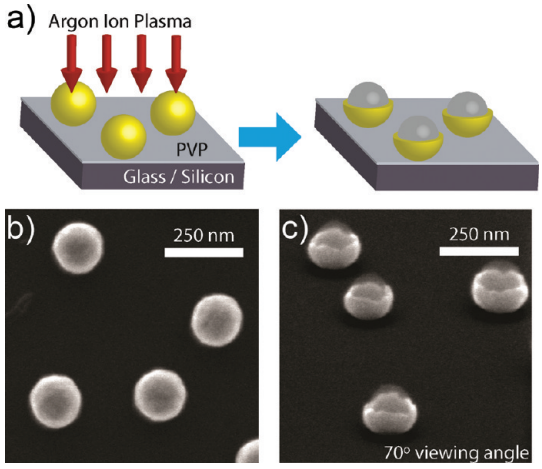

Figure 1. Fabrication of nanoparticle samples. (a) Pristine substrate (either glass or silicon) was functionalized with PVP and submerged in an aqueous solution of gold–silica nanoshells to immobilize the particles on the surface. To fabricate nanocups, the sample was then exposed to a high power argon plasma etch. The top half of the gold shell was ablated, leaving a nanocup oriented in the direction of the surface normal. SEM micrographs of (b) nanoshells before and (c) oriented nanocups after the etching process.

(Figure 1b). Images obtained at an oblique angle (70°) show that hemispherical nanoparticles are formed in this manner, where the rim of each nanocup contains small random height fluctuations (Figure 1c).

Analysis of the nanoparticle optical properties was performed using a commercial finite element method software package (COMSOL Multiphysics 4.2, RF Module). A nanoshell was modeled as two concentric spheres of radii $[r_1, r_2]$ = [60, 78] nm, consistent with the dimensions of the nanoshells used in the experiments. Nanocups with a smooth rim were modeled by removing the upper half of the gold shell layer and leaving the silica core intact. The bottom of each particle was modeled with a 3 nm facet, to allow for appropriate meshing of the numerical simulation and placed in direct contact with a semi-infinite substrate. Scattering spectra were obtained by using the Stratton–Chu formula[34] to calculate the far-field from a well-defined near-field boundary and then integrating over the cross section accessible to the collection assembly at each position on the rotating stage.

Extinction measurements (Varian CARY 5000 UV–vis–NIR spectrophotometer) of nanocups and nanoshells allow us to directly compare the plasmonic properties of the etched nanocups with the spherically symmetric nanoshells from which they were obtained (Figure 2). Here the nanoshells were deposited on transparent glass substrates to facilitate the optical extinction measurements. The samples were placed at an angle of 45° with respect to the incident light, and P-polarized incident light was used to correspond to our light-scattering measurements. The nanoshell has one principal dipolar plasmon mode (Figure 2a).[6,35,36] Three-fold degeneracy, as illustrated by charge

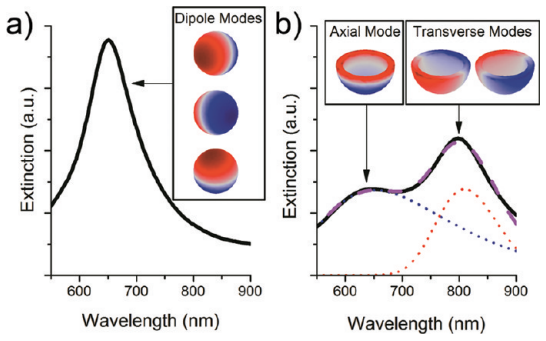

Figure 2. Extinction measurements of nanoshells and nanocups on a glass substrate, oriented at 45°. P-polarized light excites the principal *l* = 1 dipole plasmon modes for (a) nanoshells and (b) nanocups. A two-peak Gaussian fit isolates the contribution of the axial mode (blue) and transverse mode (red) of the nanocup extinction spectrum of nanocups. Insets show simulated charge distributions obtained using FEM modeling, showing the qualitative orientation of the electric dipole for each plasmon mode in a homogeneous environment.

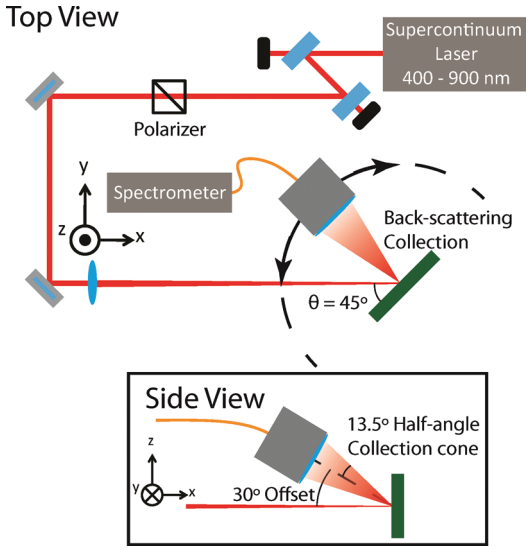

Figure 3. Schematic of the backscattering detection system. An attenuated commercial supercontinuum laser (400−900 nm) was polarized and focused onto a sample ($\theta = 45°$). A rotational stage equipped with a collection lens and fiber coupler rotates around the sample to measure the far-field radiation. Side view: Scattered light was collected from 30° above the plane of the table to prevent the collection optics from obstructing the incident beam or becoming saturated by specular reflection. The collected light is fiber-coupled into a spectrometer for analysis from 550 to 900 nm.

distributions, due to the symmetry of the nanoparticle, allows this dipole mode to be excited by both S- and P-polarized incident light (Figure 2a inset). As expected, the orientation of the electric dipole moment of the plasmon mode is solely controlled by the incident direction and polarization of light. Under P-polarized light, the degeneracy has been shown to be partially lifted, where the energy of one mode is redshifted by the presence of the dielectric substrate.[37,38]

In contrast, the reduced symmetry of the etched nanocup creates two types of orthogonal dipole plasmons with respect to the single axis of symmetry (Figure 2b). The higher-energy, axial mode is centered at nominally 650 nm for the specific dimensions used in these experiments and is characterized by charges oscillating along the axis of symmetry, from the rim to the bottom of the semishell. The two lower-energy, degenerate transverse modes are categorized as magnetic plasmon modes because charges oscillate from one side of the rim to the opposite side following the curvature of the metal.[23] Because the nanocup is an asymmetric particle, there is no axis of symmetry in the net electron motion and the net result is an optical frequency magnetic resonance. For the dimensions used here, the wavelength of these transverse modes varied between 800 and 850 nm between samples, due to the sensitivity to the etching process during fabrication. For this nanocup orientation, the axial mode is perpendicular to the substrate surface, while the two transverse modes are parallel to the substrate surface. An incident angle of 45° with respect to the surface normal was chosen to simultaneously excite both the axial and transverse modes of the nanocup: S-polarized light excites only one transverse mode, while P-polarized light excites both the axial and the other transverse mode. This geometry allows us to study the angular and spectral dependence of light scattered from both modes of the nanocup without varying the incident illumination angle.

Nanoparticle Scattering Profiles. A custom-built detection system was used to measure the scattering profile of nanoparticles as a function of polarization, scattering angle, and wavelength (Figure 3). Light from a commercial supercontinuum laser source (Fianium SC400) was passed through a spatial filter and Glan-Taylor polarizer before being focused onto the sample. The samples were mounted vertically in the center of a rotating stage such that the laser was incident upon the sample at 45 ± 2° with respect to the surface normal. A collection assembly consisting of an achromatic lens and commercial fiber collimation package was mounted on the rotating stage. This experimental configuration gathers scattered light in a 13.5° half-angle collection cone, rotated in 5° increments around the normal vector of the sample surface. In order to achieve a large collection range (75° on either side of the normal vector), the collection assembly was oriented 30° above the incident beam to avoid obstructing the beam and collecting light from specular reflection at the interface (Figure 3, inset). Backscattered light from the sample was coupled into a multimode fiber and passed to a commercial spectrometer (Ocean Optics USB4000-VIS-NIR) for analysis.

Our angle- and wavelength-dependent measurements of nanoshells and nanocups on a glass substrate are shown in Figure 4. For a dipole nanoantenna in a homogeneous medium ($\varepsilon_{substrate} = 1$), with S-polarized

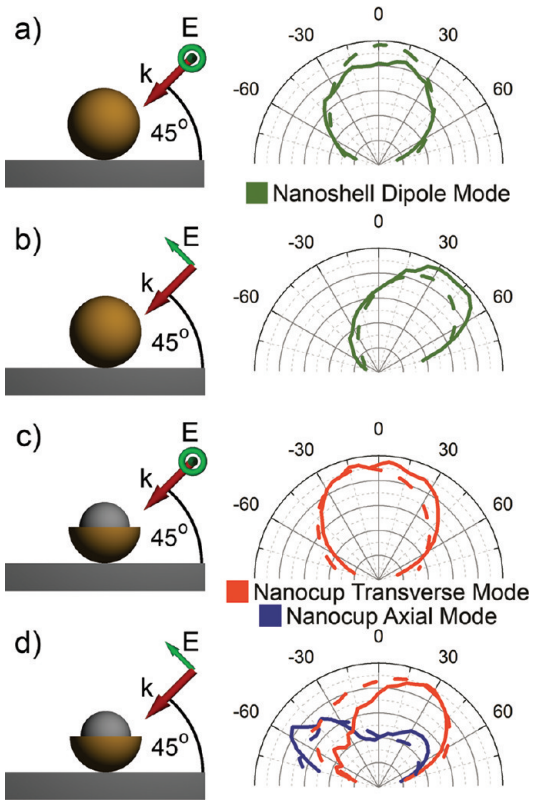

Figure 4. Angular dependence of far-field scattering from nanoshell and nanocup plasmon modes on glass substrates. The amplitude of the Gaussian distribution for each mode is plotted as a function of detector position with respect to the surface normal (0°). Experimental (solid) and theoretical (dashed) data are plotted for the case of light incident at +45° with S- or P-polarization indicated by the inset schematics. (a) Scattering of S-polarized light by a nanoshell (λ = 650 nm). (b) Scattering of P-polarized by a nanoshell (λ = 650 nm). (c) Scattering of S-polarized light by an upright nanocup (λ = 850 nm). (d) P-polarized light incident on a nanocup excites both the transverse (λ = 850 nm) and the axial (λ = 675 nm) plasmon modes.

incident light, this collection assembly would measure a uniform intensity at all angles, due to the cylindrical symmetry of the dipole radiation pattern. P-polarized incident light would yield the expected $\cos^2\theta$ intensity pattern, with maximum intensity along the axis of the incident light. The presence of a substrate ($\varepsilon_{substrate} > 1$) in the system imposes boundary conditions on the electromagnetic field at the interface. These conditions create a dark zone in the angular region close to the substrate where light cannot radiate into the far field, but instead refracts into the supporting substrate.[39−41] This property is observed for nanoshells on a glass (ε_{glass} = 2.5) substrate for S-polarized incident light (Figure 4a). For P-polarized light incident on the same substrate-supported nanoshell sample, a dipolar scattering pattern is observed in the backscattered light (Figure 4b).

In contrast to symmetric nanoparticles, the reduced symmetry of the nanocup "locks" the orientation of the oscillating electric dipole with respect to the nanocup axis of symmetry. Incident light at 45° excites a combination of the two transverse modes or the single axial mode, allowing us to observe the angle-dependent light scattering from all plasmon modes of the nanoparticle, for different polarizations of the incident light. For S-polarized incident light, the electric field couples to the transverse nanocup mode oriented perpendicular to the reflection plane (Figure 4c). The measured intensity of the transverse mode, centered at 825 nm, is maximal at 0° with respect to the surface normal and falls to zero as the detector approaches the plane of the substrate. The majority of scattered light is radiated away from the substrate or refracted into the substrate at an angle $\theta < \theta_c$, the critical angle for total internal reflection (TIR). A portion of the total energy radiated above, but also along, the interface couples into the substrate, as evident by the observation of the same dark zone discussed above.

For P-polarized incident light, a component of the incident field excites the transverse mode parallel to both the reflectance plane and the substrate surface. Simulations predict that this should result in light scattering normal to the substrate. However, in this case of the nanocups used here, the experimental scattering profile is slightly asymmetric but remains within the predicted envelope. The remaining component of the electric field, oriented normal to the surface, excites the axial nanocup mode. For this mode, the oscillating dipole is now oriented normal to the substrate and produces the expected dipole scattering pattern along the plane of the interface (Figure 4d). It is critical to note that this scattering is due to the nanocup geometry and not coupling to a high-dielectric substrate,[17,18] as the dielectric constant of glass (ε_{glass} = 2.5) produces a weak image charge.

Effect of Nanocup Geometry. Examining the spectral dependence in addition to the angular dependence of scattered light from nanocups reveals more aspects of their mode-dependent far-field properties. Two-dimensional maps of both the wavelength (*y*-axis) and angle (*x*-axis) dependence of the scattered light from nanocups are shown in Figure 5. Experimental measurements of our samples yielded a two-dimensional map with both spectrally and angularly distinct scattering from the axial and transverse modes (Figure 5a). Theoretical simulations of this spectral and angular dependence show that in our experimental system, a red shift is preferentially observed for the transverse plasmon modes (Figure 5b). Such a red shift of the transverse mode cannot be caused by the interaction with the substrate because the axial mode is expected to exhibit a much larger substrate-induced red shift than the transverse mode.[37,38] To further investigate this red shift, we now examine how the detailed geometry of the nanocup rim influences its scattering properties.

Here we observe that the precise nanoscale geometry of the nanocup plays a significant role in

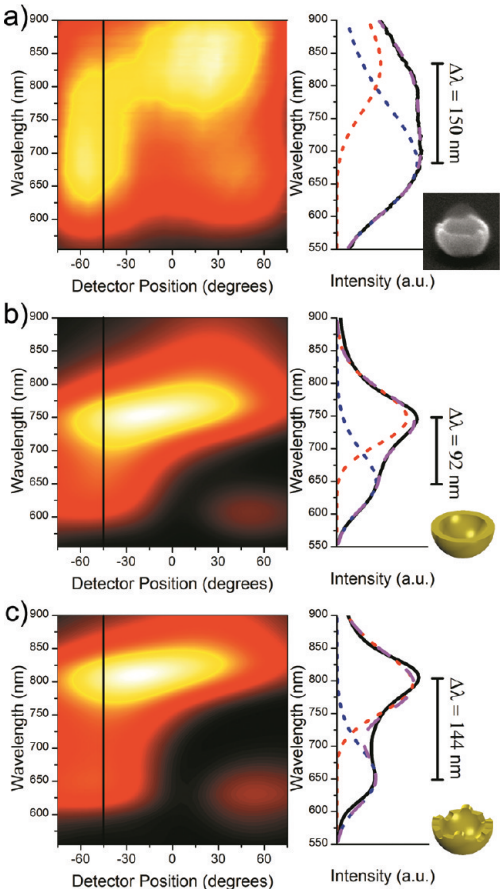

Figure 5. Effect of nanocup geometry on plasmon mode energies. (a) Left: experimental scattering profile (color) of a nanocup on a glass substrate plotted as a function of detector position (*x*-axis) and wavelength (*y*-axis). Incident light was P-polarized and illuminated the sample from +45°. Right: plot of the scattered spectrum at −45° showing Gaussian peaks for the axial (blue) and transverse (red) modes. (b) Simulated smooth rim nanocup shows the same qualitative scattering features but reduced mode separation. (c) By adding an oscillatory rim to the simulated nanocup, the separation of the two nanocup modes increases by approximately 50 nm, similar to the experimentally measured mode separation.

determining the resonant wavelength of each plasmon mode. To more accurately simulate the experimental morphology of the etched nanocups, an oscillatory rim with the same thickness as the original gold layer was superimposed on the simple nanocup. The addition of this wavering edge geometry allows the collective oscillation of electrons in the transverse plasmon to produce higher charge densities in the sharp features of the new rim (Figure 5c). This increases the polarizability of the transverse modes, red-shifting them by approximately 50 nm, closer to the experimentally observed values. Because the charges at the circular rim would still remain evenly distributed with this new geometry, the axial mode does not shift appreciably due to this rim structure. The net effect of the change in geometry is an increase in the relative separation of the axial and transverse modes. The change in rim geometry does not reorient the dipole moment of either plasmon mode, so the angular dependence of the scattering profile remains unaffected. Other minor deviations between theory and experiment are due to the ensemble-based measurement of the nanoparticles, which includes a random distribution of nanocups with these slight irregularities in the rim.

Effects of Substrate Permittivity. To further investigate the optical properties of a nanocup under the influence of a dielectric substrate, combined spectral and angular scattering measurements were performed for etched nanocups on a silicon substrate. Figure 6 presents the idealized case of nanocups deposited directly on a pristine, non-oxidized silicon substrate ($\varepsilon_{silicon}$ = 11.69) and illuminated with P-polarized light (Figure 6a). Simulations predict an overall drop in scattering intensity (Figure 6b) relative to lower permittivity substrates, which is consistent with recent investigations of enhanced collection efficiency due to the deposition of plasmonic nanostructures on the input face of photodetectors and photovoltaic devices.[15,42] The angular dependence of scattering (Figure 6c) is expected to be completely dominated by backscattering at the incident angle of illumination (+45°), mimicking the localized scattering behavior of P-polarized light on a spherically symmetric nanoshell. This profile is a consequence of strong coupling of the plasmon modes of a nanoparticle with the high permittivity substrate through interaction with its image charge.[37]

In the image charge model, the magnitude of the image charge is modified by a factor proportional to $(\varepsilon - 1)/(\varepsilon + 1)$, which approaches unity for high-dielectric materials, such as silicon. Interaction with this image charge is more prominent with the axial plasmon mode (Figure 6e, left) due to the charge distribution along the axis of symmetry, specifically, the proximity of the charges at the bottom of the nanocup and the image charge projected on the surface of the substrate. The image dipole is aligned with the nanoparticle dipole, resulting in a larger net dipole and increased coupling with the incident radiation. The transverse mode (Figure 6e, center) is weakly affected since charges localized on the rim of the nanocup are well-separated from their image charges on the substrate. In this case, the image and nanoparticle dipoles are oppositely oriented, weakening the net dipole moment of the system. Thus, in the presence of high-dielectric substrates, the energy of the axial plasmon mode is red-shifted toward the energy of the transverse plasmon mode, and the separation of the resonant wavelengths of each respective mode is greatly reduced (Figure 6b).

In the case of 45° incidence and P-polarized light, the combination of both of these complex interactions explains the predicted scattering profile for 725 nm light (Figure 6c) and can also give rise to higher order

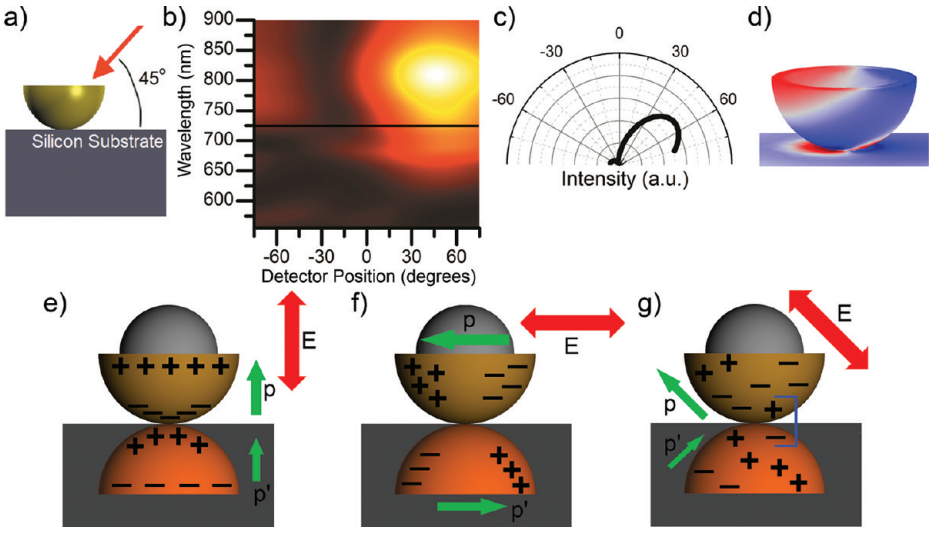

Figure 6. Effects of a pristine silicon substrate on the plasmon spectrum and angular light scattering of a nanocup. (a) Schematic of nanocup/substrate simulation space with P-polarized light illuminating the sample from +45°. (b) Scattering profile (color intensity) of a nanocup on a silicon substrate plotted as a function of detector position (*x*-axis) and wavelength (*y*-axis). (c) In polar coordinates (degrees), the angular distribution of 725 nm scattered light is strongly localized in the direction of backscattering, dictated by orientation of the charge distribution (d) on the nanocup. (e) Qualitative orientation of surface charge on the nanocup and the image charge within the substrate for purely axial [left], purely transverse [center], and the experimental [right] polarization of incident light. The green arrows depict the orientation of the effective dipole moment of the nanocup, p, and the image charge distribution, p′.

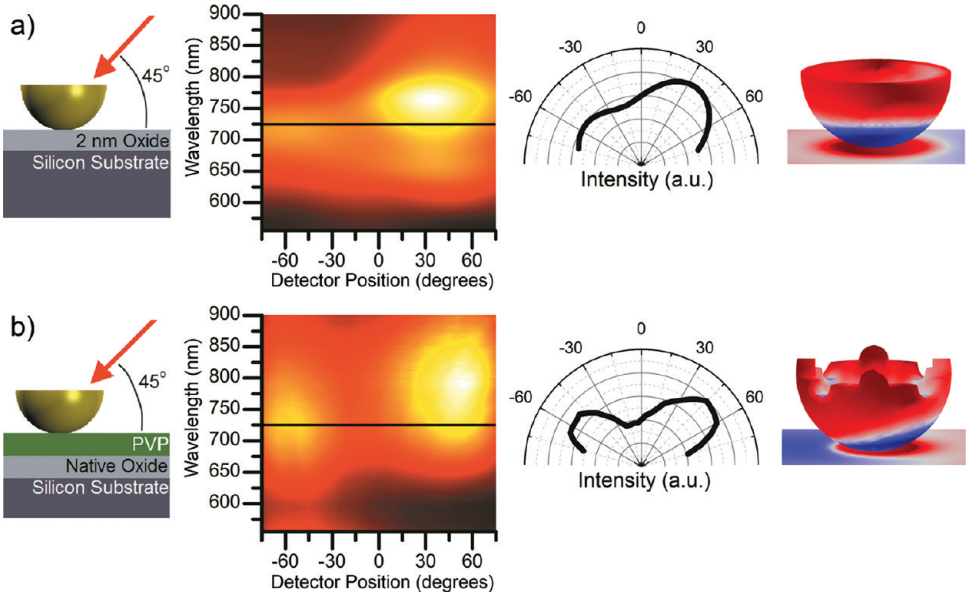

Figure 7. Effects of a realistic silicon substrate on the plasmon spectrum and angular light scattering of a nanocup. In each panel is displayed (left to right): schematic of nanocup illumination and geometry of silicon substrate; scattering profile (color intensity) of a nanocup on a silicon substrate plotted as a function of detector position (*x*-axis) and wavelength (*y*-axis); angular distribution of 725 nm scattered light in polar coordinates (degrees); and charge distribution of the nanocup. In all cases, incident light is P-polarized and illuminates the sample from +45°. (a) Simulation: the addition of a 2 nm thick low-dielectric layer (ε_{film} = 2.50) atop the silicon substrate blue shifts the plasmon modes. A forward-scattering peak in the direction of specular reflection (−45°) begins to emerge in the angular scattering distribution. The charge distribution on the nanocup is now dominated by the axial mode. (b) Experiment: The native oxide/PVP layer on the silicon surface results in a blue-shifting of the plasmon modes and the emergence of both a forward and backward scattering lobe, consistent with simulations in (a). The (theoretical) charge distribution of a nanocup with an oscillatory rim retains its primarily axial mode character.

($n > 1$) plasmon modes. The charge distribution on the nanocup (Figure 6d) indicates that the principle nanocup modes, now with similar plasmon energies, have hybridized to form a net dipole oriented along the polarization of the incident laser. The image dipole of the nanocup produces an inhomogeneous electric field in the near-field region of the nanocup, allowing hybridization with higher order plasmon modes,

demonstrated by the appearance of a faint linear quadrupole with an axis of symmetry aligned with the polarization of incident light. As a result, the charge distribution has a net dipole moment oriented along the polarization of the incident electric field. The radiation from this dipole explains the strong localized scattering observed in the direction of incidence (+45°). While the resonant wavelength for this mode is located around 825 nm, the scattering profile at 725 nm exhibits the same features and permits comparison of this idealized system with the more advanced model described below.

When a nanoscale dielectric layer is incorporated into the basic model (Figure 7a), we observe marked differences in the angular scattering spectra of the nanoparticle which provides useful insight into the properties of our experimental system. The addition of this dielectric more accurately reflects our experimental system (Figure 7b) which includes both a nanoscale native oxide layer and a nanoscale polymer layer to facilitate adhesion of the nanoparticles to the substrate. The simulation space was altered by including a 2 nm layer with an effective dielectric constant of ε_{film} = 2.50 between the nanocup and underlying substrate. Compared to the case of pristine silicon, the presence of a low-dielectric layer slightly blue shifts the axial plasmon mode away from the transverse modes and back toward the original resonance at 675 nm on glass. The angular dependence, however, indicates an entirely new scattering pattern compared to that of pristine silicon (Figure 6c). The presence of this low-dielectric barrier between the nanocup and the silicon creates two interfaces, deviating from the simple image charge model. Despite the extremely small thickness of the low-dielectric film, the effect on the scattering profile is significant in our experimental characterization of this system. While the strongest scattering remains primarily in the direction of incidence (+45°), there is now, in addition, a significant amplitude of forward scattering in the direction of specular reflection (−45°). This is facilitated by the original nanocup axial mode which completely dominates the transverse and quadrupolar contributions. This study shows that small, highly localized changes in the dielectric of an underlying substrate may have large effects on the light-scattering properties of nanocups, a property that may provide a useful route to active control of light-scattering properties.

CONCLUSIONS

In this study, we have examined the spectral- and angle-dependent light-scattering properties of plasmonic nanocups, through experimental studies and numerical simulations. The transverse and axial plasmon modes of a nanocup scatter light in distinct angular patterns that are sensitive to the presence of a dielectric substrate and its local permittivity adjacent to the nanoparticle. On low-dielectric substrates, both the axial and transverse nanocup modes scatter light in directions determined by nanocup orientation. With a high degree of sensitivity, the permittivity of the underlying substrate affects not only the wavelength of the resonances but also the angular light scattering of the system in significant ways. The different angular scattering and wavelength response from the axial and transverse nanocup modes make the nanocup an interesting particle for the nanoscale manipulation of light in three dimensions. The sensitivity of this system to geometric and environmental factors may present opportunities for active, substrate-mediated control of light scattering.

METHODS

Nanocup Fabrication. Fabrication of nanocups involved exposing nanoshells immobilized on a glass or silicon substrate to an argon plasma etch in a Trion Minilock-Phantom III reactive ion etch (RIE). The samples were placed inside an etching chamber pressurized to 80 mTorr with a flow rate of 100 sccm (standard cubic centimeters per minute) of Ar gas. The plasma was triggered and maintained by the RF generator (13.56 MHz) operating at 300 W. The inductively coupled plasma (ICP) power source of the unit was not utilized for this fabrication process. The high power settings resulted in an etching process dominated by the physical ablation of the gold nanoshell by accelerated argon ions. Etching was oriented perpendicularly into the surface of the substrate and progressively removed the gold shell from the top edge. The samples were etched for 45 s to achieve nominal nanocup geometry (Figure 1c).

Finite Element Method (FEM) Modeling. All simulations were performed using the COMSOL 4.2 RF module (commercial FEM software). A spherical simulation space was surrounded with a perfectly matched layer (PML) to absorb scattered light and then a scattering boundary condition to prevent reflections. The space, including the PML regions, was divided by a plane to simulate the dielectric interface of the supporting substrate. The dielectric constant, $\varepsilon_{substrate}$, for the bottom hemisphere was chosen to reflect the appropriate substrate used in the experiment (ε_{glass} = 2.50, $\varepsilon_{silicon}$ = 12.69), while the upper hemisphere was modeled as air, ε_{air} = 1.00. An effective oxide layer was modeled as a second interface with a constant thickness and with a dielectric constant of ε_{oxide} = 2.50. The incident radiation was defined as a simple monochromatic plane wave incident at 45° that satisfied the Fresnel equations at the dielectric interface. This approach counters the major reflections between the interface and PML layers. The simulation space does not implement periodic boundary conditions, which represent a perfect array as opposed to the randomly oriented particles in the experiment.

A nanoshell was modeled as two concentric spheres of radius [r_1, r_2] = [60, 78] nm at the center of the simulation space. The optical constants of the Au outer shell were described using experimental values[43] and the silica core as an isotropic dielectric with ε_{core} = 2.04. To model a simple nanocup, the upper half of the Au shell was removed, leaving a Au semishell with a smooth rim. A model created to more accurately simulate the structure of the fabricated nanocups involved adding and removing semicircular (radius 15 nm) patches of gold with the same thickness as the original shell to and from the smooth rim

(see Supporting Information Figure S1). This wavering edge is a representative geometry of the inhomogeneous rim that results from the plasma etching process. At the bottom of each particle, a 3 nm facet was created to properly model the curvature of the nanoparticle coming into contact with the flat substrate surface.

For a reasonable approximation of the far-field radiation patterns, a near-field to far-field transformation[34] was performed in postprocessing by performing on a well-defined surface around the nanoparticle. Because of the supporting substrate, the transformation surface is hemisphere exclusively above the interface. For each detector position and simulated wavelength, the far-field intensity was integrated inside the angular region of this transform surface that corresponded to the collection cone of the optical assembly (Figure 3). Electric field plots (see Supporting Information Figure S2) easily identify the localized field enhancements and plasmonic hot-spots. Charge plots were generated by applying Gauss's Theorem at the surface of the particle. The difference between the orthogonal component of the electric field immediately above and below the metal surface within an infinitely small pillbox was calculated to obtain the surface charge density. The phase of the incident wave was adjusted to find the maximum amplitude of the resonant charge oscillations of the plasmon modes (see Supporting Information Figure S3).

Acknowledgment. We would like to thank N. Mirin, J. B. Lassiter, M. Knight, K. Bao, R. Huschka, J. Day, and S. Lal for technical and editorial support. This research was supported by the Center for Advanced Solar Photophysics, an Energy Frontier Research Center funded by the U.S. Department of Energy, Office of Basic Energy Sciences (78506-001-09) and the Robert A. Welch Foundation (C-1220 and C-1222).

Supporting Information Available: SEM images of nanocup rim morphology and simulated geometry for nanocup with wavering rim; scattered electric field intensity cross-sectional plot for nanocups and nanoshells; charge plots of nanocup modes at a single wavelength. This material is available free of charge *via* the Internet at http://pubs.acs.org.

REFERENCES AND NOTES

1. Chen, X.; Li, S.; Xue, C.; Banholzer, M. J.; Schatz, G. C.; Mirkin, C. A. Plasmonic Focusing in Rod-Sheath Heteronanostructures. *ACS Nano* **2009**, *3*, 87–92.
2. Hartstein, A.; Kirtley, J. R.; Tsang, J. C. Enhancement of the Infrared Absorption from Molecular Monolayers with Thin Metal Overlayers. *Phys. Rev. Lett.* **1980**, *45*, 201–204.
3. Moskovits, M. Surface-Enhanced Spectroscopy. *Rev. of Mod. Phys.* **1985**, *57*, 783–826.
4. Schmelzeisen, M.; Zhao, Y.; Klapper, M.; Müllen, K.; Kreiter, M. Fluorescence Enhancement from Individual Plasmonic Gap Resonances. *ACS Nano* **2010**, *4*, 3309–3317.
5. Shegai, T.; Brian, B.; Miljković, V. D.; Käll, M. Angular Distribution of Surface-Enhanced Raman Scattering from Individual Au Nanoparticle Aggregates. *ACS Nano* **2011**, *5*, 2036–2041.
6. Oldenburg, S. J.; Averitt, R. D.; Westcott, S. L.; Halas, N. J. Nanoengineering of Optical Resonances. *Chem. Phys. Lett.* **1998**, *288*, 243–247.
7. Preston, T. C.; Signorell, R. Growth and Optical Properties of Gold Nanoshells Prior to the Formation of a Continuous Metallic Layer. *ACS Nano* **2009**, *3*, 3696–3706.
8. Zhang, L.; Wang, H. Cuprous Oxide Nanoshells with Geometrically Tunable Optical Properties. *ACS Nano* **2011**, *5*, 3257–3267.
9. Hentschel, M.; Dregely, D.; Vogelgesang, R.; Giessen, H.; Liu, N. Plasmonic Oligomers: The Role of Individual Particles in Collective Behavior. *ACS Nano* **2011**, *5*, 2042–2050.
10. Stender, A. S.; Wang, G.; Sun, W.; Fang, N. Influence of Gold Nanorod Geometry on Optical Response. *ACS Nano* **2010**, *4*, 7667–7675.
11. Pillai, S.; Catchpole, K. R.; Trupke, T.; Zhang, G.; Zhao, J.; Green, M. A. Enhanced Emission from Si-Based Light-Emitting Diodes Using Surface Plasmons. *Appl. Phys. Lett.* **2006**, *88*, 161102.
12. Chang, C.-C.; Sharma, Y. D.; Kim, Y.-S.; Bur, J. A.; Shenoi, R. V.; Krishna, S.; Huang, D.; Lin, S.-Y. A Surface Plasmon Enhanced Infrared Photodetector Based on InAs Quantum Dots. *Nano Lett.* **2010**, *10*, 1702–1709.
13. Yu, E. T.; Derkacs, D.; Lim, S. H.; Matheu, P.; Schaadt, D. M. Plasmonic Nanoparticle Scattering for Enhanced Performance of Photovoltaic and Photodetector Devices. *Proc. SPIE* **2008**, *7033*, 70331V.
14. Atwater, H. A.; Polman, A. Plasmonics for Improved Photovoltaic Devices. *Nat. Mater.* **2010**, *9*, 205–213.
15. Catchpole, K. R.; Polman, A. Plasmonic Solar Cells. *Opt. Express* **2008**, *16*, 21793–21800.
16. Aubry, A.; Lei, D. Y.; Maier, S. A.; Pendry, J. B. Plasmonic Hybridization between Nanowires and a Metallic Surface: A Transformation Optics Approach. *ACS Nano* **2011**, *5*, 3293–3308.
17. Chen, H.; Ming, T.; Zhang, S.; Jin, Z.; Yang, B.; Wang, J. Effect of the Dielectric Properties of Substrates on the Scattering Patterns of Gold Nanorods. *ACS Nano* **2011**, *5*, 4865–4877.
18. Chen, S.-Y.; Mock, J. J.; Hill, R. T.; Chilkoti, A.; Smith, D. R.; Lazarides, A. A. Gold Nanoparticles on Polarizable Surfaces as Raman Scattering Antennas. *ACS Nano* **2010**, *4*, 6535–6546.
19. Hu, Y. S.; Jeon, J.; Seok, T. J.; Lee, S.; Hafner, J. H.; Drezek, R. A.; Choo, H. Enhanced Raman Scattering from Nanoparticle-Decorated Nanocone Substrates: A Practical Approach To Harness In-Plane Excitation. *ACS Nano* **2010**, *4*, 5721–5730.
20. Otte, M. A.; Estevez, M.-C.; Carrascosa, L. G.; Gonzalez-Guerro, A. B.; Lechuga, L. M.; Sepulveda, B. Improved Biosensing Capability with Novel Suspended Nanodisks. *J. Phys. Chem. C* **2011**, *115*, 5344–5351.
21. Sherry, L. J.; Chang, S.-H.; Schatz, G. C.; Van Duyne, R. P. Localized Surface Plasmon Resonance Spectroscopy of Single Silver Nanocubes. *Nano Lett.* **2005**, *5*, 2034–2038.
22. Swanglap, P.; Slaughter, L. S.; Chang, W.-S.; Willingham, B.; Khanal, B. P.; Zubarev, E. R.; Link, S. Seeing Double: Coupling between Substrate Image Charges and Collective Plasmon Modes in Self-Assembled Nanoparticle Superstructures. *ACS Nano* **2011**, *5*, 4892–4901.
23. Cortie, M.; Ford, M.; Plasmon-Induced Current, A Loop in Gold Semi-Shells. *Nanotechnology* **2007**, *18*, 235704.
24. Mirin, N. A.; Halas, N. J. Light-Bending Nanoparticles. *Nano Lett.* **2009**, *9*, 1255–1259.
25. Ye, J.; Van Dorpe, P.; Van Roy, W.; Lodewijks, K.; De Vlaminck, I.; Maes, G.; Borghs, G. Fabrication and Optical Properties of Gold Semishells. *J. Phys. Chem. C* **2009**, *113*, 3110–3115.
26. Ye, J.; Verellen, N.; Van Roy, W.; Lagae, L.; Maes, G.; Borghs, G.; Van Dorpe, P. Plasmonic Modes of Metallic Semishells in a Polymer Film. *ACS Nano* **2010**, *4*, 1457–1464.
27. Chang, W.-S.; Ha, J. W.; Slaughter, L. S.; Link, S. Plasmonic Nanorod Absorbers as Orientation Sensors. *Proc. Natl. Acad. Sci. U.S.A.* **2010**, *107*, 2781–2786.
28. Cubukcu, E.; Zhang, S.; Park, Y.-S.; Bartal, G.; Zhang, X. Split Ring Resonator Sensors for Infrared Detection of Single Molecular Monolayers. *Appl. Phys. Lett.* **2009**, *95*, 043113.
29. Liu, N.; Kaiser, S.; Giessen, H. Magnetoinductive and Electroinductive Coupling in Plasmonic Metamaterial Molecules. *Adv. Mater.* **2008**, *20*, 4521–4525.
30. Zhang, Y.; Barhoumi, A.; Lassiter, J. B.; Halas, N. J. Orientation-Preserving Transfer and Directional Light Scattering from Individual Light-Bending Nanoparticles. *Nano Lett.* **2011**, *11*, 1838–1844.
31. Brinson, B. E.; Lassiter, J. B.; Levin, C. S.; Bardhan, R.; Mirin, N. A.; Halas, N. J. Nanoshells Made Easy: Improving Au Layer Growth on Nanoparticle Surfaces. *Langmuir* **2008**, *24*, 14166–14171.
32. Malynych, S.; Luzinov, I.; Chumanov, G. Poly(vinyl pyridine) as a Universal Surface Modifier for Immobilization of Nanoparticles. *J. Phys. Chem. B* **2002**, *106*, 1280–1285.
33. Mirin, N. A.; Ali, T. A.; Nordlander, P.; Halas, N. J. Perforated Semishells: Far-Field Directional Control and Optical Frequency Magnetic Response. *ACS Nano* **2010**, *4*, 2701–2712.

34. Stratton, J. *Electromagnetic Theory*; McGraw-Hill: New York, 1941.
35. Oldenburg, S. J.; Jackson, J. B.; Westcott, S. L.; Halas, N. J. Infrared Extinction Properties of Gold Nanoshells. *Appl. Phys. Lett.* **2001**, *75*, 2897–2899.
36. Tam, F.; Chen, A. L.; Kundu, J.; Wang, H.; Halas, N. J. Mesoscopic Nanoshells: Geometry-Dependent Plasmon Resonances Beyond the Quasistatic Limit. *J. Chem. Phys.* **2007**, *127*, 204703.
37. Knight, M. W.; Wu, Y.; Lassiter, J. B.; Nordlander, P.; Halas, N. J. Substrates Matter: Influence of an Adjacent Dielectric on an Individual Plasmonic Nanoparticle. *Nano Lett.* **2009**, *9*, 2188–2192.
38. Wu, Y.; Nordlander, P. Finite-Difference Time-Domain Modeling of the Optical Properties of Nanoparticles near Dielectric Substrates. *J. Phys. Chem. C* **2010**, *114*, 7302–7307.
39. Arnoldus, H. F.; Foley, J. T. Transmission of Dipole Radiation through Interfaces and the Phenomenon of Anti-Critical Angles. *J. Opt. Soc. Am.* **2004**, *21*, 1109–1117.
40. Lukosz, W.; Kunz, R. E. Light Emission by Magnetic and Electric Dipoles Close to a Plane Dielectric Interface. II. Radiation Patterns of Perpendicular Oriented Dipoles. *J. Opt. Soc. Am.* **1977**, *67*, 1615–1619.
41. Novotny, L.; Hecht, B. *Principles of Nano-Optics*; Cambridge University Press: Cambridge, 2006.
42. Sundararajan, S. P.; Grady, N. K.; Mirin, N.; Halas, N. J. Nanoparticle-Induced Enhancement and Suppression of Photocurrent in a Silicon Photodiode. *Nano Lett.* **2008**, *8*, 624–630.
43. Johnson, P. B.; Christy, R. W. Optical Constants of the Noble Metals. *Phys. Rev. B* **1972**, *6*, 4370–4379.